THE JOURNAL OF PHYSICAL CHEMISTRY Letters

Letter

Cite This: J. Phys. Chem. Lett. 2019, 10, 6455−6461

pubs.acs.org/JPCL

Effect of Atomic Corrugation on Adhesion and Friction: A Model Study with Graphene Step Edges

Zhe Chen,[†,§] Mohammad R. Vazirisereshk,[‡,§] Arash Khajeh,[‡] Ashlie Martini,*[,‡] and Seong H. Kim*[,†]

[†]Department of Chemical Engineering and Materials Research Institute, Pennsylvania State University, University Park, Pennsylvania 16802, United States

[‡]Department of Mechanical Engineering, University of California Merced, Merced, California 95343, United States

Supporting Information

ABSTRACT: This Letter reports that the atomic corrugation of the surface can affect nanoscale interfacial adhesion and friction differently. Both atomic force microscopy (AFM) and molecular dynamics (MD) simulations showed that the adhesion force needed to separate a silica tip from a graphene step edge increases as the side wall of the tip approaches the step edge when the tip is on the lower terrace and decreases as the tip ascends or descends the step edge. However, the friction force measured with the same AFM tip moving across the step edge does not positively correlate with the measured adhesion, which implies that the conventional contact mechanics approach of correlating interfacial adhesion and friction could be invalid for surfaces with atomic-scale features. The chemical and physical origins for the observed discrepancy between adhesion and friction at the atomic step edge are discussed.

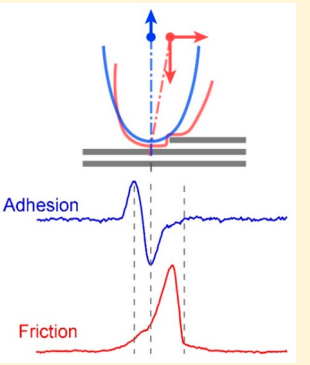

Interfacial adhesion plays an important role in a variety of applications from the nanoscale to the macroscale, such as surface coatings for engineering materials,[1,2] synthesis of composite materials,[3,4] and filtration of particulates from water and air.[5,6] Adhesion also plays a significant role in friction at the nanoscale because adhesion affects the size of the contact between two bodies.[7−9] Friction is often modeled as shear stress times contact area.[10−12] If the contact is elastic and the shear stress term is assumed to be constant,[11,12] then experimentally measured friction forces can be related to the contact area. The contact area can be mathematically modeled as a function of the effective elastic moduli and radii of the contacting bodies, and the sum of the applied normal force and the adhesion force.[13,14] Then, the shear stress of the sliding contact can be empirically obtained by dividing the measured friction by the calculated contact area, and its magnitude can be related to the surface chemistry of materials.[7,15,16] Thus, knowing the adhesion behavior of the contacting interface can provide critical insights into interfacial friction processes.

Although such analysis is widely employed in friction and adhesion studies,[7,17,18] other studies have reported that friction and adhesion exhibit opposite trends.[19−21] Therefore, fundamental questions remain about how closely interfacial adhesion can be correlated to friction. Experimentally, adhesion is determined by measuring the force needed to separate contacting bodies while applying a tensile stress to the contact along the direction normal to the interface. In contrast, the friction force is measured by shearing along the tangential direction of the interface with an applied compressive force. Because they are obtained separately and in different measurement modes, experimentally observed adhesion and friction trends may not always be positively correlated through the contact area argument.

Here, we investigated the nanoscale adhesion and friction behaviors of a silica probe on an atomically flat surface with well-defined topographic steps. Atomic step edges on graphite surfaces were chosen for this study because both topographic and chemical properties of these steps are well-known: (i) terraces are the atomically flat and chemically inert carbon surface, (ii) step heights are multiples of the single-layer graphene thickness (0.34 nm), and (iii) step edges exposed to air are terminated with C−OH and C−H groups.[22−25] Also, there are a large number of experimental and computational studies of friction at graphene step edges for comparison with the adhesion behavior observed and explained in this study.[24−34] Here, our AFM and MD simulation results demonstrate local variation of adhesion at step edges and provide insights into how atomic-scale topographic corrugations affect the adhesion force measurement. Then, comparison of the topography-dependent adhesion with friction at the same step edge suggests that these two are not always positively correlated to each other. The chemical and physical origins for the discrepancy between these two properties are discussed.

Received: August 26, 2019
Accepted: October 4, 2019
Published: October 4, 2019

DOI: 10.1021/acs.jpclett.9b02501
J. Phys. Chem. Lett. 2019, 10, 6455−6461

Figure 1a shows the topography of an 800 nm by 800 nm area on a freshly exfoliated graphite surface that contains four

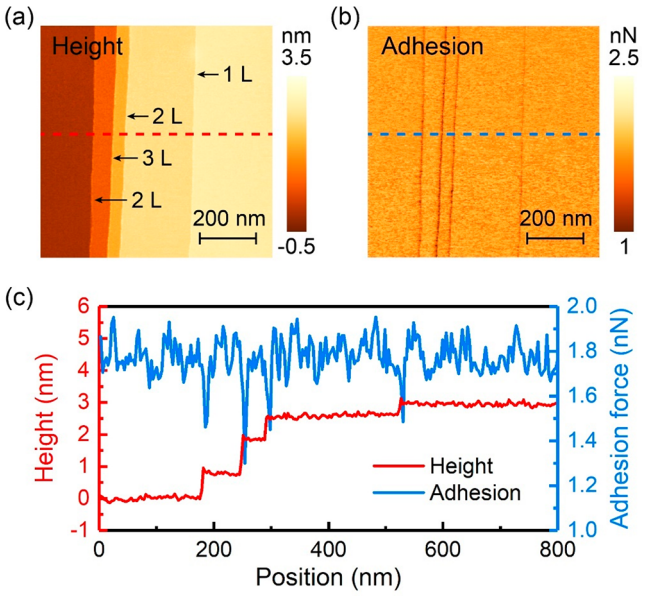

Figure 1. Topography and adhesion on a freshly exfoliated graphite surface. (a) Height and (b) adhesion force maps collected simultaneously on an 800 nm by 800 nm region containing four exposed step edges with different heights (different numbers of graphene layers). (c) Line traces of the height and the adhesion force along the dashed lines in (a) and (b), respectively.

step edges. According to the height change, these four edges, from left to right in the image, comprise 2, 3, 2, and 1 layer (L) graphene. At all four step edges, the friction force increases during both step-up and step-down processes (see Figure S1), indicating that these step edges are exposed to the air and not covered by graphene layers.[24,26,28,33] The adhesion force of the same region collected simultaneously with the topography is shown in Figure 1b. The topography and adhesion along a line perpendicular to the step edges are shown in Figure 1c, and a sharp drop in the adhesion can be observed at each of the four step edges.

To further investigate the adhesion force at the exposed step edges, high-resolution scanning was performed near the 1, 2, and 3 L steps. The topography and adhesion maps obtained when the AFM tip was scanning from left to right in these regions are shown in Figure 2a,b, respectively. The data obtained during the scan in the opposite direction were the same (not shown). The average height and adhesion profiles are shown in Figure 2c. The three step edges exhibit similar adhesion trends, despite their height difference. When the AFM tip is on the lower terrace far from the step edge, the adhesion force on the basal plane is measured to be 1.8 nN. When the AFM tip approaches the step and begins to ascend, both the recorded topographic height and adhesion increase gradually. When the adhesion force reaches a maximum value (position A in the 1 L panel of Figure 2c), the recorded height begins to increase sharply; in contrast, the adhesion force starts decreasing, although the recorded height continues to increase. At position B in the 1 L panel of Figure 2c, the recorded height is at a maximum, but the adhesion force is a minimum. Finally, as the recorded height decreases to the position of the upper terrace, the adhesion force increases to a value slightly larger than the basal plane value (position C) and then returns to the basal plane value (~1.8 nN) when the tip is entirely on the upper terrace. Note that the magnitude of the adhesion depends on the environment, but the same trends are observed in air and in dry N_2 (see Figure S2). These trends are also similar to those observed in the previous work of Stifter et al.,[35] in which the measurement of adhesion at multilayer graphene step edges was performed in an electrolyte solution. Note that other AFM-based studies have reported no change in the adhesion at graphene step edges of various heights in dry N_2,[36] humid[28] and ambient[31] conditions. Unless the data were collected with sufficiently high spatial resolution with low signal-to-noise ratio, subtle changes near or at the step edges may not have been evident.

For the height profiles displayed in Figure 2c, the initial and final values (at 0 and 20 nm) indicate the relative heights of the lower terrace and the upper terrace; therefore, the difference between them, ΔH_1, is the absolute height of the step edge. The height difference between the upper terrace and the highest point (position B) in the height profile is labeled ΔH_2. The values of ΔH_1 and ΔH_2 for all three step edges with different heights are reported in Figure 3a. ΔH_1 increases stepwise from ~0.34 to ~0.68 nm and then to ~1.02 nm, consistent with the expected heights of multiple layers of graphene. The value of ΔH_2 does not vary with the number of layers and is recorded as ~0.2 nm for all three step edges.

The adhesion forces far from the step on either side in Figure 2c are the same, corresponding to the adhesion force on the graphite basal plane. The difference between the adhesion on the basal plane and the first maximum that occurs when the tip is adjacent to the step on the lower terrace (position A), the minimum when the tip is at the step (position B), and the second maximum when the tip is adjacent to the step on the upper terrace (position C) are labeled ΔF_1, ΔF_2, and ΔF_3, respectively, in the 3 L panel of Figure 2c. The values of ΔF_1, ΔF_2, and ΔF_3 for the three step edges are reported in Figure 3b. Similar to ΔH_1, the magnitudes of both ΔF_1 and ΔF_2 increase with the number of graphene layers. ΔF_3 remains constant and very small for all step edges analyzed.

Note that ΔH_2 at position B and ΔF_3 at position C are not always observed (see Figure S2). In previous studies, it was proposed that the topographic feature at the step edge (ΔH_2) may be due to rupture, buckling, or grafting of functional groups at the graphene step edge.[23,25,30,32] If these events occur, ΔH_2 and ΔF_3 could be attributed to the interaction between the protruded part at the step edge and the back side of the tip. However, this could not be confirmed from the experimental data.

Considering that the native oxide of the AFM Si tip is hydrophilic and the step edge has hydroxyl groups,[23,37] one may speculate if a capillary bridge could be formed at the step edge and have an impact on the adhesion force measured in humid conditions.[38,39] However, the adhesion measured in dry N_2 exhibits the same behavior observed in ambient air (see Figure S2). The adhesion force in ambient air is slightly larger than that in dry N_2, which could be attributed to the water adsorption on the tip surface.[40] There is no water adsorption on the pristine graphite surface; even at the step edge, physisorption of water is extremely small in relative humidity less than 90%.[24] Finally, to confirm that the trends are not the result of a capillary, simulations were performed with an atomistic simulation of a model tip apex and graphite surface in vacuum.

DOI: 10.1021/acs.jpclett.9b02501
J. Phys. Chem. Lett. 2019, 10, 6455−6461

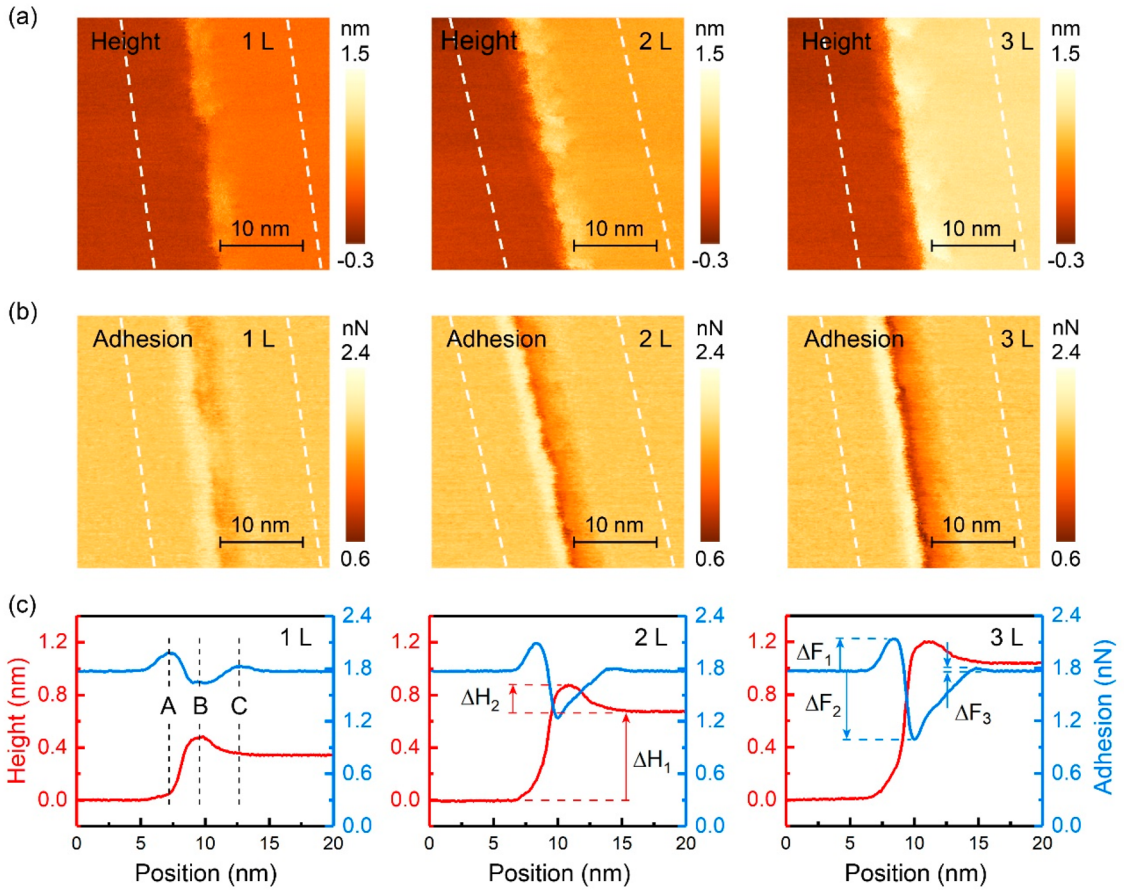

Figure 2. Effect of the number of graphene layers on adhesion at exposed step edges. (a) Topography of three 30 nm by 30 nm regions, which contain 1, 2, and 3 L graphene step edges. (b) Adhesion force in the same regions. Line traces (c) show the average height (red lines) and the average adhesion force (blue lines) of the data in the regions between the two dashed lines in (a) and (b). Position A refers to the position of the highest adhesion force. Position B refers to the position of the lowest adhesion force. Position C refers to the position where the tip starts to be fully on the upper terrace. The definition of positions A, B, and C remains the same in the following figures. The meanings of ΔH and ΔF are discussed in the text.

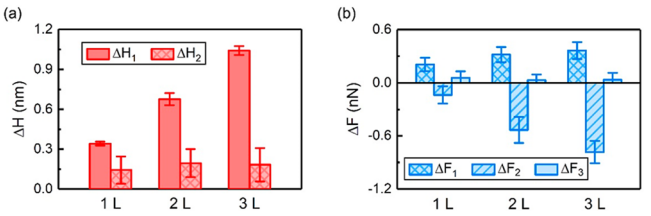

Figure 3. (a) Height of the step edge (ΔH_1) and the height difference between the highest point and the upper terrace (ΔH_2). (b) Adhesion at the two peaks (ΔF_1 and ΔF_3) and one valley (ΔF_2) relative to the average adhesion on terraces.

The MD simulations mimicked an AFM adhesion measurement on 1, 2, and 3 L graphene step edges (Figures S3 and S4). The simplified model, in which the tip and the graphite surface interacted only via van der Waals forces, reduced the simulation time and enabled quantitative analysis of how the atomic-height step affects interfacial adhesion without complications from chemical interactions involving functional groups at the step edge or physiosorbed molecules.[24,25] The simulated height and adhesion profiles are shown in Figure 4. The MD simulation results exhibit trends similar to those observed in the experiments shown in Figure 2c. The adhesion increases when the tip approaches the step edge from the lower terrace (ΔF_1) and the adhesion decreases when the tip is ascending the step edge (ΔF_2) are clearly observed in the simulation (see Figure S5 for the value of ΔF_1 and ΔF_2). Higher adhesion when the tip moves from the step edge onto the upper terrace (ΔF_3) is not observed, likely due to the simplified simulation structure that does not contain defects or functional groups.[22−25] Regardless, these results, obtained from simulations in ideal vacuum, confirm that the trends are independent of capillary effects.

To understand the origin of the nonmonotonic adhesion trend, the contributions of the front (facing the step edge) and back halves of the model tip are analyzed separately (see 1 L panels in Figure 4). This analysis shows that, on the basal plane and far from the step edge, both the front and back halves of the tip contribute equally to the total adhesion. As the tip approaches the step edge from the lower terrace, the adhesion of the front part of the tip increases slightly due to additional van der Waals interactions with the step edge, while the back-side adhesion remains constant, resulting in a slight increase in the overall adhesion, quantified by ΔF_1 (at position A). As the tip ascends the step, the interactions between the surface and both the front and back halves of the tip decrease. The back-side contribution decreases more significantly because it is far from the lower terrace at this moment. This decrease is directly related to the minimum adhesion force (ΔF_2), which is observed when the center of the tip is on the lower terrace

DOI: 10.1021/acs.jpclett.9b02501
J. Phys. Chem. Lett. 2019, 10, 6455−6461

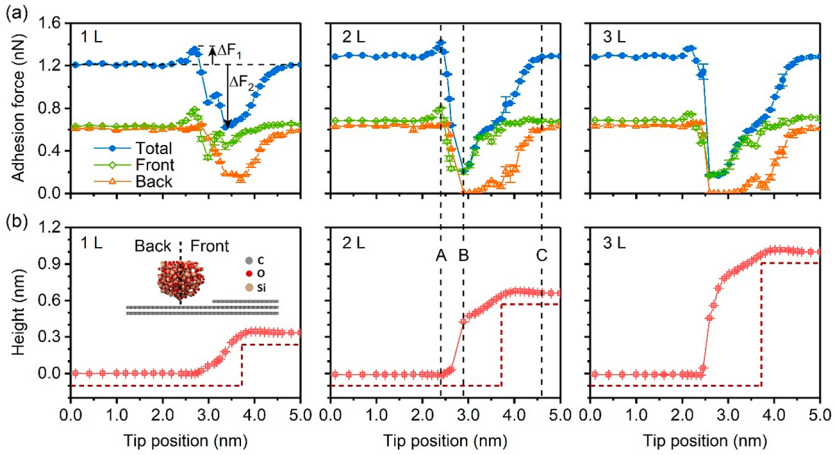

Figure 4. (a) Adhesion and (b) height from MD simulations of adhesion tests at 1, 2, and 3 L step edges. In (a), the total adhesion (solid blue circles) is broken down into contributions from the front (hollow green diamonds) and back (hollow orange triangles) of the tip. The red dashed lines in (b) represent the real shape of the step edges corresponding to the positions of the atoms in the simulation. Error bars for the values are mostly hidden behind the symbols. The inset in (b) shows the simulation setup for 1 L with the front and back parts of the tip identified.

side. At position B, the tip is farthest from the two terraces. For larger tips, the ΔF_2 position is farther from the step, as confirmed by the simulations shown in Figure S6. Moreover, as shown in Figure S7, the contact area between the tip and the graphite substrate has the same trends as the adhesion force, as expected. However, as soon as the tip retraction begins, the contact area starts to decrease until it reaches zero (see Figures S4 and S7), indicating that the contact condition at the moment when the adhesion is measured is different from that when the tip is in equilibrium with the graphite substrate. Lastly, in Figure 4b, there is a slight overshoot in the simulated height after the tip moves onto the upper terrace. The magnitude of this overshoot is independent of the tip geometry (see Figure S6) and appears to be associated with the larger vibration amplitude of the carbon atoms at the step edge.[25] However, it was difficult to determine if this is directly relevant to the ΔH_2 observed in the AFM PeakForce QNM imaging (Figure 2c).

With deeper understanding of how atomic corrugations (step edges) influence the adhesion force measured for the nanoscale single asperity contact using AFM, we can now study whether friction positively correlates with adhesion on the same surface. Figure 5 shows the adhesion force, lateral force, and height profiles obtained with a single AFM tip moving across a 1 L thick graphene step edge. In Figure 5a, the adhesion force on the graphite basal plane is about 7.4 nN, indicating that the AFM tip used for this measurement is not as sharp as the one used for the data shown in Figure 2, but the trend of the adhesion force across the graphene step edge is the same. The lateral force signals obtained with the same AFM tip (Figure 5b) are consistent with previously reported data.[24,25] Friction at a graphene step edge is governed by two components: (i) a geometric effect due to the topographic height change at the step edge and (ii) a chemical effect due to the interactions between the tip and the step edge.[24,25] Previous simulations with a reactive force field showed that the topographic effect originates from the elastic deformation of the AFM tip and leads to a resistive force during the step-up motion and an assistive force during the step-down motion, while the chemical effect is associated with hydrogen bonding between the AFM tip and hydroxyl groups terminating the graphene step edge and results in a resistive force during both

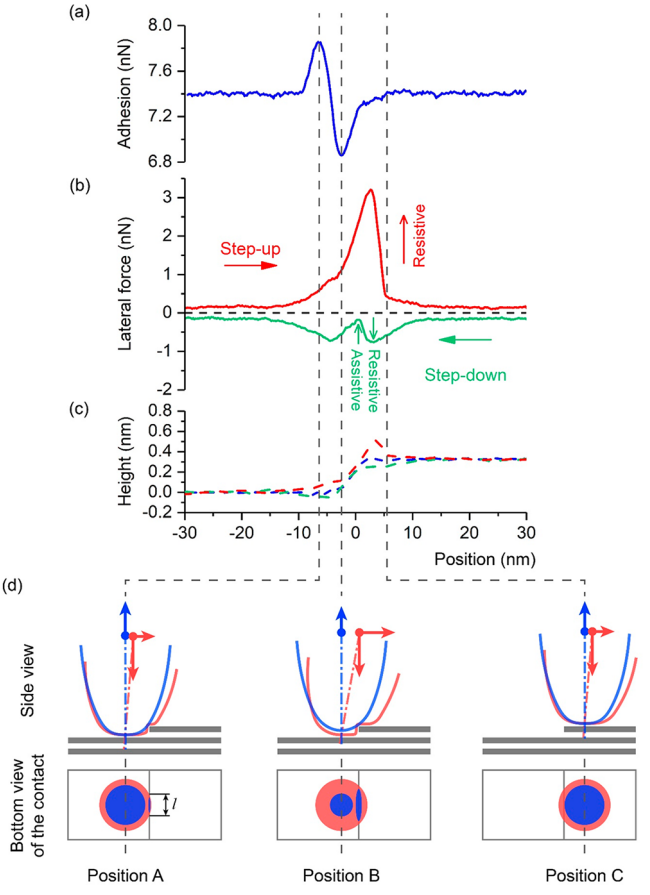

Figure 5. (a) Adhesion force, (b) lateral force (step-up in red, step-down in green), and (c) height profile obtained with the same AFM tip sliding over a 1 L graphene step edge. (d) Tilting and deformation of the tip during adhesion measurement (blue) and friction measurement (red) at positions A, B, and C. The arrows in (d) represent the force from the AFM probe cantilever to the AFM tip. The lateral force was measured with an applied normal load of about 7 nN.

step-up and step-down motion.[24,25] The shape of the friction profile is the same in vacuum and ambient conditions,[24] because the water adsorption on the AFM tip surface and at

DOI: 10.1021/acs.jpclett.9b02501
J. Phys. Chem. Lett. 2019, 10, 6455−6461

graphene step edges is not sufficient to form a capillary meniscus.

By aligning the adhesion and lateral force data in reference to the recorded height data (Figure 5c), it can be seen that they do not correlate positively with each other. This same trend is observed in the simulations (Figure S8). As mentioned previously, the friction force is measured while applying compressive and shear stresses to the interfacial contact, and the adhesion force is measured while applying vertical tensile force to the contact. This is schematically illustrated in Figure 5d, showing the deformation and tilting of the AFM tip and the contact area between the tip and the graphite surface. During the step-up motion, when the tip is at position A, the vertical adhesion force is the largest because of the additional contact of the tip side wall with the step edge. At this point, the lateral friction force just starts increasing from the basal plane value because interactions between the tip side wall and the step edge begin to contribute. As the tip moves from position A to position B, the vertical force needed to separate the contact (which is measured as the "adhesion force" in AFM) decreases because the effective contact area at the snap-off moment decreases (Figure S7); in contrast, the torque exerted by the step edge on the tip (which is recorded as "lateral friction" in AFM) increases because the total resistance to the contact sliding increases in proportion to the contact length between the tip and the step edge (l; see Figure 5d). At position B, the vertical adhesion is the lowest, but the lateral friction is large. At this position, the geometric contribution to the step-up friction increases drastically because the tip center is now crossing the step edge and moving toward the upper terrace. According to previous reports, as the tip is lifted from the lower terrace to the upper terrace, the tip surface deformation decreases significantly; at the same time, the chemical contribution also decreases because the contact length l decreases.[24,25] Once the tip moves onto the upper terrace, the vertical adhesion force increases as the contact area between the back side of the tip and the upper terrace increases at the moment of snap-off. Note that the positions of the minimum adhesion and the maximum friction recorded in AFM do not match. This is because the AFM records the position of the cantilever to which the tip is attached (solid dots in the side view of Figure 5d), not the position of the tip end interacting with the surface.

For the step-down motion of the AFM tip from the upper terrace to the lower terrace, the tip deformation and chemical interactions in the contact area region are the same as the step-up motion case, but the titling direction of the tip is opposite, and negative lateral force refers to resistive force. For the measurement shown in Figure 5b, the assistive topographic effect is not as strong as the resistive chemical effect.[24,25] Because the directions of the tip−surface interactions are different between the step-up and step-down motion, the friction behavior depends on the scan direction. By contrast, the vertical adhesion force measured through the PeakForce Tapping mode is not a function of scan direction.

The results shown in Figure 5 question the validity of applying the conventional contact mechanics concepts to friction at atomic-height step edges. In conventional contact mechanics,[10,41] the adhesion force is viewed as an additional contribution to the total normal force experienced by the tip. This is reasonable because adhesion increases the compressive stress in the contact area. In practice (especially in AFM experiments), the adhesion force used in theoretical calculations of the contact area is measured as the force needed to separate the contact between two surfaces (which is called "pull-off" or "snap-off" force) while a tensile stress is applied in the surface normal direction. The data in Figure 5 clearly show that the adhesion force measured while pulling the tip vertically from the surface can vary independently from the friction force measured while compressing the tip and shearing it laterally along the surface. Note that this does not mean that the conventional contact mechanics are incorrect, but it does imply that the contribution of adhesion to friction may not be properly calculated if the pull-off force is used as the adhesion force in theoretical calculations, even for relatively flat surfaces with only atomic-height corrugations. This issue would be most significant when the interfacial adhesion is weak and the surface is not compliant. For large adhesion and/or highly compliant contacting materials (like polymers or self-assembled organic layers), the error from using the pull-off force in the contact area calculation might be smaller.[42,43]

The friction data in Figure 5b also suggest that the local shear stress within the contact area on an atomically corrugated surface would not be constant due to physical (elastic) deformation of the contacting surfaces. Within the contact, the compressive stress would be different on the upper and lower terraces as well as at the step edge.[44] The situation becomes much more complicated when there are functional groups present at the step edge (and other topographically corrugated surfaces) that can induce chemical interactions. In the absence of any chemical effect, which is the case for a covered graphene step edge,[24] the topographic effect of the atomic-height step is small and fully reversible; the magnitude in friction increase during step-up motion is the same as the friction decrease during step-down motion. However, in the presence of chemical interactions, the resistive force during the step-up is significantly larger than the assistive force during the step-down.[25] The shear stress determined from the continuum contact mechanics analysis[8−10,41] must be an average of all topographic and chemical processes occurring at atomic corrugations inside of the contact area.

In summary, the effect of atomic-height corrugations (graphene step edges) on the adhesion force and friction force was reported based on AFM measurements and MD simulations. The high-resolution adhesion measurements reveal that adhesion force exhibits significant local variations (up to 45% variation from the terrace value) near the step. Further, it was found that the adhesion force and the lateral force at the same atomic corrugation are not positively correlated with each other. This observation indicates that, in the presence of surface corrugation, it may not be appropriate to correlate the contact area calculated from pull-off test adhesion measurements (obtained under tensile stress) to friction measured during sliding under compressive and tangential shear stress. This finding has important implications for interpreting friction measurements obtained using AFM and, more generally, for understanding friction at the nanoscale where adhesive forces play a significant, if not dominant, role in determining the observed behavior.

■ ASSOCIATED CONTENT

Supporting Information

The Supporting Information is available free of charge on the ACS Publications website at DOI: 10.1021/acs.jpclett.9b02501.

DOI: 10.1021/acs.jpclett.9b02501
J. Phys. Chem. Lett. 2019, 10, 6455−6461

Materials and methods for both experiments and simulations; additional experimental results, including friction and adhesion from measurements in air and in dry N_2 (Figures S1 and S2); and detailed simulation results, including model schematics, time-dependent data, adhesion obtained using a larger model tip, contact size, and direct comparison between adhesion and lateral force (Figures S3–S8) (PDF)

AUTHOR INFORMATION

Corresponding Authors

*E-mail: amartini@ucmerced.edu (A.M.).
*E-mail: shkim@engr.psu.edu (S.H.K.).

ORCID

Zhe Chen: 0000-0002-5874-7196
Mohammad R. Vazirisereshk: 0000-0001-8122-7749
Arash Khajeh: 0000-0002-9061-9370
Ashlie Martini: 0000-0003-2017-6081
Seong H. Kim: 0000-0002-8575-7269

Author Contributions

§Z.C. and M.R.V. contributed equally.

Notes

The authors declare no competing financial interest.

ACKNOWLEDGMENTS

This work was supported by the National Science Foundation (Grant No. CMMI-1727571 and 1727356).

REFERENCES

(1) Cemin, F.; Boeira, C. D.; Figueroa, C. A. On the Understanding of the Silicon-Containing Adhesion Interlayer in DLC Deposited on Steel. *Tribol. Int.* **2016**, *94*, 464–469.
(2) Santiago, J. A.; Fernández-Martínez, I.; Wennberg, A.; Molina-Aldareguia, J. M.; Castillo-Rodríguez, M.; Rojas, T. C.; Sánchez-López, J. C.; González, M. U.; García-Martín, J. M.; Li, H.; Bellido-González, V.; Monclús, M. A.; González-Arrabal, R. Adhesion Enhancement of DLC Hard Coatings by Hipims Metal Ion Etching Pretreatment. *Surf. Coat. Technol.* **2018**, *349*, 787–796.
(3) Liu, Y.; Zhang, X.; Song, C.; Zhang, Y.; Fang, Y.; Yang, B.; Wang, X. An Effective Surface Modification of Carbon Fiber for Improving the Interfacial Adhesion of Polypropylene Composites. *Mater. Des.* **2015**, *88*, 810–819.
(4) Budhe, S.; Banea, M. D.; de Barros, S.; da Silva, L. F. M. An Updated Review of Adhesively Bonded Joints in Composite Materials. *Int. J. Adhes. Adhes.* **2017**, *72*, 30–42.
(5) Wisser, D.; Wisser, F. M.; Raschke, S.; Klein, N.; Leistner, M.; Grothe, J.; Brunner, E.; Kaskel, S. Biological Chitin–MOF Composites with Hierarchical Pore Systems for Air-Filtration Applications. *Angew. Chem., Int. Ed.* **2015**, *54*, 12588–12591.
(6) Shin, S.; Shardt, O.; Warren, P. B.; Stone, H. A. Membraneless Water Filtration Using CO_2. *Nat. Commun.* **2017**, *8*, 15181.
(7) Noy, A.; Frisbie, C. D.; Rozsnyai, L. F.; Wrighton, M. S.; Lieber, C. M. Chemical Force Microscopy: Exploiting Chemically-Modified Tips to Quantify Adhesion, Friction, and Functional Group Distributions in Molecular Assemblies. *J. Am. Chem. Soc.* **1995**, *117*, 7943–7951.
(8) Johnson, K. L.; Kendall, K.; Roberts, A. Surface Energy and the Contact of Elastic Solids. *Proc. R. Soc. London, Ser. A* **1971**, *324*, 301–313.
(9) Derjaguin, B. V.; Muller, V. M.; Toporov, Y. P. Effect of Contact Deformations on the Adhesion of Particles. *J. Colloid Interface Sci.* **1975**, *53*, 314–326.
(10) Mo, Y.; Turner, K. T.; Szlufarska, I. Friction Laws at the Nanoscale. *Nature* **2009**, *457*, 1116.
(11) Riedo, E.; Chevrier, J.; Comin, F.; Brune, H. Nanotribology of Carbon Based Thin Films: The Influence of Film Structure and Surface Morphology. *Surf. Sci.* **2001**, *477*, 25–34.
(12) Szlufarska, I.; Chandross, M.; Carpick, R. W. Recent Advances in Single-Asperity Nanotribology. *J. Phys. D: Appl. Phys.* **2008**, *41*, 123001.
(13) Grierson, D. S.; Flater, E. E.; Carpick, R. W. Accounting for the JKR–DMT Transition in Adhesion and Friction Measurements with Atomic Force Microscopy. *J. Adhes. Sci. Technol.* **2005**, *19*, 291–311.
(14) Jacobs, T. D. B.; Martini, A. Measuring and Understanding Contact Area at the Nanoscale: A Review. *Appl. Mech. Rev.* **2017**, *69*, 060802.
(15) Kwon, S.; Ko, J.-H.; Jeon, K.-J.; Kim, Y.-H.; Park, J. Y. Enhanced Nanoscale Friction on Fluorinated Graphene. *Nano Lett.* **2012**, *12*, 6043–6048.
(16) Berman, D.; Erdemir, A.; Zinovev, A. V.; Sumant, A. V. Nanoscale Friction Properties of Graphene and Graphene Oxide. *Diamond Relat. Mater.* **2015**, *54*, 91–96.
(17) Koren, E.; Lörtscher, E.; Rawlings, C.; Knoll, A. W.; Duerig, U. Adhesion and Friction in Mesoscopic Graphite Contacts. *Science* **2015**, *348*, 679.
(18) Maeda, N.; Chen, N.; Tirrell, M.; Israelachvili, J. N. Adhesion and Friction Mechanisms of Polymer-on-Polymer Surfaces. *Science* **2002**, *297*, 379.
(19) Vazirisereshk, M. R.; Ye, H.; Ye, Z.; Otero-de-la-Roza, A.; Zhao, M.-Q.; Gao, Z.; Johnson, A. T. C.; Johnson, E. R.; Carpick, R. W.; Martini, A. Origin of Nanoscale Friction Contrast between Supported Graphene, MoS_2, and a Graphene/MoS_2 Heterostructure. *Nano Lett.* **2019**, *19*, 5496–5505.
(20) Ptak, F.; Almeida, C. M.; Prioli, R. Nanoscale Friction of Graphene. *MRS Adv.* **2018**, *3*, 2743–2748.
(21) Yoshizawa, H.; Chen, Y. L.; Israelachvili, J. Fundamental Mechanisms of Interfacial Friction. 1. Relation between Adhesion and Friction. *J. Phys. Chem.* **1993**, *97*, 4128–4140.
(22) Rietsch, J.-C.; Brender, P.; Dentzer, J.; Gadiou, R.; Vidal, L.; Vix-Guterl, C. Evidence of Water Chemisorption During Graphite Friction under Moist Conditions. *Carbon* **2013**, *55*, 90–97.
(23) Levita, G.; Restuccia, P.; Righi, M. C. Graphene and MoS_2 Interacting with Water: A Comparison by *ab initio* Calculations. *Carbon* **2016**, *107*, 878–884.
(24) Chen, L.; Chen, Z.; Tang, X.; Yan, W.; Zhou, Z.; Qian, L.; Kim, S. H. Friction at Single-Layer Graphene Step Edges Due to Chemical and Topographic Interactions. *Carbon* **2019**, *154*, 67–73.
(25) Chen, Z.; Khajeh, A.; Martini, A.; Kim, S. H. Chemical and Physical Origins of Friction on Surfaces with Atomic Steps. *Sci. Adv.* **2019**, *5*, eaaw0513.
(26) Hölscher, H.; Ebeling, D.; Schwarz, U. D. Friction at Atomic-Scale Surface Steps: Experiment and Theory. *Phys. Rev. Lett.* **2008**, *101*, 246105.
(27) Egberts, P.; Ye, Z.; Liu, X. Z.; Dong, Y.; Martini, A.; Carpick, R. W. Environmental Dependence of Atomic-Scale Friction at Graphite Surface Steps. *Phys. Rev. B: Condens. Matter Mater. Phys.* **2013**, *88*, 035409.
(28) Lang, H.; Peng, Y.; Zeng, X.; Cao, X. a.; Liu, L.; Zou, K. Effect of Relative Humidity on the Frictional Properties of Graphene at Atomic-Scale Steps. *Carbon* **2018**, *137*, 519–526.
(29) Panigrahi, S.; Bhattacharya, A.; Bandyopadhyay, D.; Grabowski, S. J.; Bhattacharyya, D.; Banerjee, S. Wetting Property of the Edges of Monoatomic Step on Graphite: Frictional-Force Microscopy and *ab initio* Quantum Chemical Studies. *J. Phys. Chem. C* **2011**, *115*, 14819–14826.
(30) Dong, Y.; Liu, X. Z.; Egberts, P.; Ye, Z.; Carpick, R. W.; Martini, A. Correlation between Probe Shape and Atomic Friction Peaks at Graphite Step Edges. *Tribol. Lett.* **2013**, *50*, 49–57.
(31) Hunley, D. P.; Flynn, T. J.; Dodson, T.; Sundararajan, A.; Boland, M. J.; Strachan, D. R. Friction, Adhesion, and Elasticity of Graphene Edges. *Phys. Rev. B: Condens. Matter Mater. Phys.* **2013**, *87*, 035417.

DOI: 10.1021/acs.jpclett.9b02501
J. Phys. Chem. Lett. 2019, 10, 6455–6461

(32) Lee, H.; Lee, H.-B.-R.; Kwon, S.; Salmeron, M.; Park, J. Y. Internal and External Atomic Steps in Graphite Exhibit Dramatically Different Physical and Chemical Properties. *ACS Nano* **2015**, *9*, 3814−3819.
(33) Ye, Z.; Martini, A. Atomic Friction at Exposed and Buried Graphite Step Edges: Experiments and Simulations. *Appl. Phys. Lett.* **2015**, *106*, 231603.
(34) Ye, Z.; Otero-de-la-Roza, A.; Johnson, E. R.; Martini, A. Effect of Tip Shape on Atomic-Friction at Graphite Step Edges. *Appl. Phys. Lett.* **2013**, *103*, 081601.
(35) Stifter, T.; Weilandt, E.; Marti, O.; Hild, S. Influence of the Topography on Adhesion Measured by SFM. *Appl. Phys. A: Mater. Sci. Process.* **1998**, *66*, S597−S605.
(36) Deng, Z.; Klimov, N. N.; Solares, S. D.; Li, T.; Xu, H.; Cannara, R. J. Nanoscale Interfacial Friction and Adhesion on Supported Versus Suspended Monolayer and Multilayer Graphene. *Langmuir* **2013**, *29*, 235−243.
(37) Cao, P.; Xu, K.; Varghese, J. O.; Heath, J. R. The Microscopic Structure of Adsorbed Water on Hydrophobic Surfaces under Ambient Conditions. *Nano Lett.* **2011**, *11*, 5581−5586.
(38) Wei, Z.; Zhao, Y.-P. Growth of Liquid Bridge in AFM. *J. Phys. D: Appl. Phys.* **2007**, *40*, 4368−4375.
(39) Megias-Alguacil, D.; Gauckler, L. J. Capillary Forces between Two Solid Spheres Linked by a Concave Liquid Bridge: Regions of Existence and Forces Mapping. *AIChE J.* **2009**, *55*, 1103−1109.
(40) Asay, D. B.; Kim, S. H. Evolution of the Adsorbed Water Layer Structure on Silicon Oxide at Room Temperature. *J. Phys. Chem. B* **2005**, *109*, 16760−16763.
(41) Johnson, K. Adhesion and Friction between a Smooth Elastic Spherical Asperity and a Plane Surface. *Proc. R. Soc. London, Ser. A* **1997**, *453*, 163−179.
(42) Yoon, E.-S.; Singh, R. A.; Oh, H.-J.; Kong, H. The Effect of Contact Area on Nano/Micro-Scale Friction. *Wear* **2005**, *259*, 1424−1431.
(43) Heim, L.-O.; Blum, J.; Preuss, M.; Butt, H.-J. Adhesion and Friction Forces between Spherical Micrometer-Sized Particles. *Phys. Rev. Lett.* **1999**, *83*, 3328−3331.
(44) Luan, B.; Robbins, M. O. The Breakdown of Continuum Models for Mechanical Contacts. *Nature* **2005**, *435*, 929.

DOI: 10.1021/acs.jpclett.9b02501
J. Phys. Chem. Lett. 2019, 10, 6455−6461